Computational Mathematics and Mathematical Physics, Vol. 38, No. 10, 1998, pp. 1662–1671.
Translated from Zhurnal Vychislitel'noi Matematiki i Matematicheskoi Fiziki, Vol. 38, No. 10, 1998, pp. 1732–1742.

Application of Quasi-Hydrodynamic Equations in the Modeling of Low-Prandtl Thermal Convection

T. G. Elizarova*, I. S. Kalachinskaya, A. V. Klyuchnikova**, and Yu. V. Sheretov*****

**Institute of Mathematical Modeling, Russian Academy of Sciences, Miusskaya pl. 4a, Moscow, 125047 Russia*

***Department of Computational Mathematics and Cybernetics, Moscow State University, Vorob'evy gory, Moscow, 119899 Russia*

****Tver State University, Tver, 170043 Russia*

Received March 3, 1998

Abstract—Results of numerical simulation are presented for buoyancy-driven and thermocapillary convection in rectangular cavities at low Prandtl numbers. The results, which were obtained by solving a quasi-hydrodynamic system of equations, are compared with the numerical results based on the Navier–Stokes equations.

INTRODUCTION

The Navier–Stokes equations are widely used to describe viscous incompressible flows. However, the construction of numerical algorithms for these equations is impeded by a number of difficulties, which mainly arise in simulations of high-speed flows. This occurs because very fine grids are necessary to resolve boundary-layer flows, specific approximations must be constructed, and regularizers are required to ensure numerical stability. Moreover, special boundary conditions must be used for pressure when the numerical algorithm is constructed for solving a set of equations written in the velocity–pressure formulation, or for vorticity when the algorithm is based on equations written in the streamfunction–vorticity formulation. In this paper, we consider an alternative approach to the numerical simulation of viscous incompressible flows, based on quasi-hydrodynamic (QHD) equations, which can be very helpful in dealing with these problems.

Systems of equations of this class were proposed for describing gas flows in [1, 2] and were called the quasi-gas-dynamic equations. These equations and the corresponding kinetically consistent difference schemes were originally derived by averaging a Boltzmann-type model equation and by analyzing the numerical algorithms designed to solve kinetic equations. In both analyses, the behavior of gas particles was treated as a cyclic process of collisionless motion followed by instant relaxation of particles to a locally Maxwellian equilibrium. The numerical algorithms based on this approach proved to be very efficient in computations of complex problems in both time-independent and transient supersonic gas dynamics. They were used in numerical analyses of pulsating flows, which play an important role in the studies of acoustic loads in real systems (see [3]).

In [4], a phenomenological derivation of a new QHD system of equations was presented. These equations differ from the classical Navier–Stokes equations by additional divergence terms. The derivation strongly relied on the assumption that the mean momentum density, $\rho\mathbf{u}$, is not equal to the mass flux, $\mathbf{j}$, in the general case. It is obvious that whether or not the vectors $\mathbf{j}$ and $\rho\mathbf{u}$ are equal depends on the averaging procedure applied to the density ρ, fluid velocity $\mathbf{u}$, and temperature T.

In the Navier–Stokes theory, the equations of fluid dynamics are constructed by smoothing over the physical space $\mathbb{R}^3_x$ at a certain moment t. At each point $(\mathbf{x}, t)$, a set M of physically infinitesimal volumes V is considered in $\mathbb{R}^3_x$. The mean values of ρ, $\mathbf{u}$, and T are assumed to be constant on M; therefore, these values can be treated as physical quantities. In changing from one inertial coordinate system to another, the spatial averages of ρ, $\mathbf{u}$, and T are transformed according to a certain law, whereas the Navier–Stokes equations, which describe their evolution, remain invariant under the Galilean group [5].

In contrast to the Navier–Stokes equations, the QHD equations describe the evolution of spatiotemporal averages of ρ, $\mathbf{u}$, and T. At each point $(\mathbf{x}, t)$, a set M_1 of physically infinitesimal volumes V_1 is considered in the phase space $\mathbb{R}^3 \times \mathbb{R}_t$. If the values of the averages are constant for every V_1 from M_1, they can be treated as physical quantities. Note that the spatiotemporal averages may change as a result of a transformation

from one inertial coordinate system to another. A detailed description of the procedure of construction of spatiotemporal averages can be found in [6]. The equation of local mass conservation must have the form

$$\partial\rho/\partial t + \operatorname{div}\mathbf{j} = 0.$$

However, it is impossible to rigorously prove that $\mathbf{j} = \rho\mathbf{u}$. The average momentum of a unit volume may change during a physically infinitesimal interval.

In [4, 6, 7], a set of exact solutions to the QHD equations was constructed, a procedure of changing to the mass Lagrangian coordinates was substantiated, the QHD equations were analyzed in the Boussinesq approximation, the properties of solutions of the type describing a stationary shock wave and the laminar boundary-layer approximation were examined, and some properties to the QHD system of equations were obtained.

Some topics concerning numerical simulation based on the QHD equations were considered in [8, 9], in particular, the well-known test problems of the isothermal incompressible flow in a square cavity with a moving top boundary, Poiseuille flow in a planar channel, buoyancy-driven convection in a laterally heated square cavity.

In this paper, we use a numerical algorithm based on the QHD equations to compute low-Prandtl buoyancy-driven and thermocapillary convective flows in rectangular cavities. In addition to the primary (steady) flow regimes, we computed secondary (unsteady) regimes. The numerical results are in good agreement with those obtained by other authors who used the Navier–Stokes model.

In the numerical analysis of the QHD equations, the problem of boundary conditions for Poisson's equation is eliminated, and a simple approximation of spatial derivatives is employed. The regularizers required to ensure numerical stability at high Grashof and Marangoni numbers are provided by the additional divergence terms with a small parameter, which appear in the equations as a result of additional smoothing over time.

1. THE SYSTEM OF QUASI-HYDRODYNAMIC EQUATIONS IN THE BOUSSINESQ APPROXIMATION

The system indicated in the section heading was derived in [4]. It can be written as

$$\operatorname{div}(\mathbf{u} - \mathbf{w}) = 0, \tag{1a}$$

$$\frac{\partial\mathbf{u}}{\partial t} + (\mathbf{u} - \mathbf{w})\nabla\mathbf{u} + \frac{1}{\rho}\nabla p = \frac{1}{\rho}\operatorname{div}\Pi - \beta\mathbf{g}T, \tag{1b}$$

$$\frac{\partial T}{\partial t} + (\mathbf{u} - \mathbf{w})\nabla T = \chi\Delta T. \tag{1c}$$

Here, $\rho = \text{const} > 0$ is the average density, $\mathbf{u} = \mathbf{u}(\mathbf{x}, t)$ is the fluid velocity, $p = p(\mathbf{x}, t)$ is the dynamic pressure, and $T = T(\mathbf{x}, t)$ is the temperature deviation from the average temperature T_0. The quantities $\mathbf{j}$ and Π are interpreted as the mass flux and viscous stress tensor, respectively, and calculated as

$$\mathbf{j} = \rho(\mathbf{u} - \mathbf{w}), \tag{2}$$

$$\Pi = \Pi_{NS} + \rho(\mathbf{u} \otimes \mathbf{w}), \tag{3}$$

where $\Pi_{NS} = \eta[(\nabla \otimes \mathbf{u}) + (\nabla \otimes \mathbf{u})^{\mathrm{T}}]$ is the Navier–Stokes viscous stress tensor,

$$\mathbf{w} = \tau\left[(\mathbf{u}\cdot\nabla)\mathbf{u} + \frac{1}{\rho}\nabla p + \beta\mathbf{g}T\right]. \tag{4}$$

In equations (1), as well as in expressions (2)–(4), the absolute viscosity η, thermal diffusivity χ, thermal expansion coefficient β, and characteristic time τ are assumed to be positive and constant; and $\mathbf{g}$ is the gravitational acceleration.

The parameter τ can be calculated (see [4]) as $\tau = \eta/(\rho c_s^2)$, where c_s is the sonic velocity in the fluid at the temperature T_0. The quantity $\rho\mathbf{u}$ is interpreted as the spatiotemporally average momentum per unit fluid volume.

In writing equations (1), we used the conventional tensor notation. In calculating the divergence of the nonsymmetric tensor Π, convolution is performed with respect to its first index.

The QHD system (1) can be rewritten in the equivalent conservative form

$$\operatorname{div}\mathbf{u} = \operatorname{div}\mathbf{w}, \tag{5a}$$

$$\frac{\partial \mathbf{u}}{\partial t} + \operatorname{div}(\mathbf{u} \otimes \mathbf{u}) + \frac{1}{\rho}\nabla p = \frac{1}{\rho}\operatorname{div}\Pi_{NS} + \operatorname{div}[(\mathbf{w} \otimes \mathbf{u}) + (\mathbf{u} \otimes \mathbf{w})] - \beta \mathbf{g} T, \tag{5b}$$

$$\partial T/\partial t + \operatorname{div}(\mathbf{u}T) = \operatorname{div}(\mathbf{w}T) + \chi \Delta T. \tag{5c}$$

As $\tau \longrightarrow 0$, it reduces to the classical Navier–Stokes equations written in the Boussinesq approximation.

In the studies of flows in closed vessels, the QHD system (5) is solved with the conventional boundary conditions for the Navier–Stokes equations, supplemented with the impermeability condition

$$(\mathbf{j} \cdot \mathbf{n})|_{\Gamma} = 0, \tag{6}$$

where $\mathbf{n} = \mathbf{n}(\mathbf{x}, t)$ is the outward unit normal to the surface Γ.

Let us write out equations (5) for planar unsteady flows in dimensionless form:

$$\frac{\partial u}{\partial x} + \frac{\partial v}{\partial y} = \tau_0 \frac{\partial}{\partial x}\left(u\frac{\partial u}{\partial x} + v\frac{\partial u}{\partial y} + \frac{\partial p}{\partial x}\right) + \tau_0 \frac{\partial}{\partial y}\left(u\frac{\partial v}{\partial x} + v\frac{\partial v}{\partial y} + \frac{\partial p}{\partial y} - \mathrm{Gr}\, T\right), \tag{7}$$

$$\begin{aligned}\frac{\partial u}{\partial t} + \frac{\partial}{\partial x}(u^2) + \frac{\partial}{\partial y}(uv) + \frac{\partial p}{\partial x} &= \frac{2}{\mathrm{Re}}\frac{\partial}{\partial x}\left(\frac{\partial u}{\partial x}\right) + \frac{1}{\mathrm{Re}}\frac{\partial}{\partial y}\left(\frac{\partial u}{\partial y}\right) + \frac{1}{\mathrm{Re}}\frac{\partial}{\partial y}\left(\frac{\partial v}{\partial x}\right)\\ + 2\tau_0 \frac{\partial}{\partial x}\left[u\left(u\frac{\partial u}{\partial x} + v\frac{\partial u}{\partial y} + \frac{\partial p}{\partial x}\right)\right] &+ \tau_0 \frac{\partial}{\partial y}\left[v\left(u\frac{\partial u}{\partial x} + v\frac{\partial u}{\partial y} + \frac{\partial p}{\partial x}\right)\right] + \tau_0 \frac{\partial}{\partial y}\left[u\left(u\frac{\partial v}{\partial x} + v\frac{\partial v}{\partial y} + \frac{\partial p}{\partial y} - \mathrm{Gr}\, T\right)\right],\end{aligned} \tag{8}$$

$$\begin{aligned}\frac{\partial v}{\partial t} + \frac{\partial}{\partial y}(v^2) + \frac{\partial}{\partial x}(uv) + \frac{\partial p}{\partial y} &= \frac{2}{\mathrm{Re}}\frac{\partial}{\partial y}\left(\frac{\partial v}{\partial y}\right) + \frac{1}{\mathrm{Re}}\frac{\partial}{\partial x}\left(\frac{\partial v}{\partial x}\right) + \frac{1}{\mathrm{Re}}\frac{\partial}{\partial x}\left(\frac{\partial u}{\partial y}\right)\\ + 2\tau_0 \frac{\partial}{\partial y}\left[v\left(u\frac{\partial v}{\partial x} + v\frac{\partial v}{\partial y} + \frac{\partial p}{\partial y} - \mathrm{Gr}\, T\right)\right] &+ \tau_0 \frac{\partial}{\partial x}\left[u\left(u\frac{\partial v}{\partial x} + v\frac{\partial v}{\partial y} + \frac{\partial p}{\partial y} - \mathrm{Gr}\, T\right)\right]\\ + \tau_0 \frac{\partial}{\partial x}\left[v\left(u\frac{\partial u}{\partial x} + v\frac{\partial u}{\partial y} + \frac{\partial p}{\partial x}\right)\right] &+ \mathrm{Gr}\, T,\end{aligned} \tag{9}$$

$$\begin{aligned}\frac{\partial T}{\partial t} + \frac{\partial}{\partial x}(uT) + \frac{\partial}{\partial y}(vT) &= \frac{1}{\mathrm{Pr}}\left(\frac{\partial^2 T}{\partial x^2} + \frac{\partial^2 T}{\partial y^2}\right) + \tau_0 \frac{\partial}{\partial x}\left[T\left(u\frac{\partial u}{\partial x} + v\frac{\partial u}{\partial y} + \frac{\partial p}{\partial x}\right)\right]\\ + \tau_0 \frac{\partial}{\partial y}\left[T\left(u\frac{\partial v}{\partial x} + v\frac{\partial v}{\partial y} + \frac{\partial p}{\partial y} - \mathrm{Gr}\, T\right)\right].\end{aligned} \tag{10}$$

Here, Re, Pr, and Gr are the Reynolds, Prandtl, and Grashof numbers, respectively; and τ_0 is the characteristic time also written in dimensionless form. The procedure of nondimensionalization of equations (7)–(10) and boundary conditions are determined by the specific problem and written out below.

2. NUMERICAL ALGORITHM

The set of equations written above was solved by a finite-difference method. The spatial derivatives in (7)–(10) were approximated on a nonuniform grid by central differences as follows:

$$\frac{\partial f}{\partial x} \approx \frac{2}{h_i + h_{i+1}}\left(\frac{f_{i+1} + f_i}{2} - \frac{f_{i-1} + f_i}{2}\right),$$

$$\frac{\partial}{\partial x}\left(\kappa\frac{\partial f}{\partial x}\right) \approx \frac{2}{h_i + h_{i+1}}\left(\kappa_{i+1/2}\frac{f_{i+1} - f_i}{h_{i+1}} - k_{i-1/2}\frac{f_i - f_{i-1}}{h_i}\right),$$

$$\frac{\partial}{\partial x}\left(\kappa\frac{\partial f}{\partial y}\right) \approx \frac{2}{h_i + h_{i+1}}\frac{2}{h_j + h_{j+1}}(\kappa_{i+1/2,\,j}(f_{i+1/2,\,j+1/2} - f_{i+1/2,\,j-1/2}) - \kappa_{i-1/2,\,j}(f_{i-1/2,\,j+1/2} - f_{i-1/2,\,j-1/2})),$$

where $x_{i+1} = x_i + h_{i+1}$, $i = \overline{1, N_1 - 1}$, $y_{j+1} = y_j + h_{j+1}$, $j = \overline{1, N_2 - 1}$, and $\kappa_{i \pm 1/2} = (\kappa_i + \kappa_{i \pm 1})/2$. All quantities were calculated at grid points. The values at half-integer grid points were calculated as the half-sums of their values at the adjacent integer grid points. Mixed derivatives were approximated in terms of their values at cell centers, which were calculated as 1/4 times the sums of their values at the adjacent grid points. Time derivatives were approximated by first-order upwind differences. The boundary of the computational

domain was located at half-integer grid points. The boundary conditions for velocity and temperature were approximated by calculating the corresponding derivatives with second-order accuracy and introducing additional layers of nonphysical grid points along the external boundaries of the computational domain.

At each time step, the pressure field was calculated by using velocity and temperature fields as a solution to Poisson's equation

$$\frac{\partial^2 p}{\partial x^2} + \frac{\partial^2 p}{\partial y^2} = \frac{1}{\tau_0}\left(\frac{\partial u}{\partial x} + \frac{\partial v}{\partial y}\right) - \frac{\partial}{\partial x}\left(u\frac{\partial u}{\partial x} + v\frac{\partial u}{\partial y}\right) - \frac{\partial}{\partial y}\left(u\frac{\partial v}{\partial x} + v\frac{\partial v}{\partial y} - \mathrm{Gr}\,T\right), \tag{11}$$

which was derived from (7) and approximated by analogy with the equations of motion. The boundary conditions for pressure were derived from impermeability condition (6) and approximated with second-order accuracy by extrapolating Poisson's equation to the boundary. Equation (11) was solved by the preconditioned generalized conjugate gradient method from [10]. The preconditioner was constructed by means of a pointwise incomplete factorization of the matrix of the linear system $A\mathbf{x} = \mathbf{B}$. The pressure at the top right point was held constant and equal to unity at all times. The convergence rate of the iterations performed in solving equation (11) determines the efficiency of the algorithm as a whole. The condition for terminating the iteration was set as follows:

$$\varepsilon_p = \left[\sum_{ij}(p_{\bar{x}x,\,ij} + p_{\bar{y}y,\,ij} + f_{ij})^2 h^2\right]^{1/2} \le 10^{-5},$$

where $-f_{ij}$ is the right-hand side of the difference counterpart of equation (11). At the next step, the velocity and temperature fields were calculated by the explicit scheme based on the difference counterparts of equations (8)–(10). A flow was considered as steady if

$$\varepsilon_u = \max_{ij}\left|\frac{u_{ij}^{n+1} - u_{ij}^{n}}{\Delta t}\right| \le 0.001,$$

where n is the number of a time step.

The numerical results are represented by isolines of the streamfunction, isotherms, isolines of velocity and pressure, and graphs of velocity evolution at several points of the computational domain. The streamfunction Ψ was calculated for the vector field $\mathbf{u} - \mathbf{w}$ satisfying the condition $\mathrm{div}(\mathbf{u} - \mathbf{w}) = 0$:

$$u - w_1 = \frac{\partial \psi}{\partial y}, \quad v - w_2 = -\frac{\partial \psi}{\partial x},$$

where $\mathbf{w} = (w_1, w_2)^{\mathrm{T}}$. When τ_0 is small, the vectors $\mathbf{u}$ and $\mathbf{u} - \mathbf{w}$ are close.

3. THERMAL CONVECTION

We considered the buoyancy-driven thermal convective flow of an incompressible fluid in a rectangular cavity of height H and length L at low Prandtl numbers Pr. This a well-known problem, which was suggested as a test for analyzing the numerical techniques designed to compute convective flows in melts. The practical utility of these computations is related to the fact that periodic temperature oscillations in metallic melts (characterized by low Prandtl numbers) poses serious problems for semiconductor crystal growth (see [11]).

The flow is described by equations (7)–(10), which can be nondimensionalized by the relations

$$x = \tilde{x}H, \quad y = \tilde{y}H, \quad u = \tilde{u}\frac{\nu}{H}, \quad v = \tilde{v}\frac{\nu}{H}, \quad t = \tilde{t}\frac{H^2}{\nu}, \quad p = \tilde{p}\rho\left(\frac{\nu}{H}\right)^2, \quad T = \tilde{T}\frac{\Delta T}{A},$$

where $A = L/H$, $\Delta T = T_1 - T_2$ is the temperature difference between the left and right walls, and $\nu = \eta/\rho$ is the kinematic viscosity. With this nondimensionalization, we have $\mathrm{Gr} = \beta g \Delta T H^4/(L\nu^2)$, $\mathrm{Re} = 1$, $\mathrm{Pr} = \nu/\chi$, and $\tau_0 = \mathrm{M}^2$, where $\mathrm{M} = \nu/(Hc_s)$ is the Mach number. The cavity has a rigid bottom, and its top boundary may be either rigid (the R–R case) or free (the R–F case).

Equations (8)–(11) are supplemented with the following boundary conditions:

bottom wall: $u = 0$, $v = 0$, $\partial p/\partial y = \mathrm{Gr}\,T$, $T(x) = A - x$;

top boundary: $u = 0$, $v = 0$, $\partial p/\partial y = \mathrm{Gr}\,T$, $T(x) = A - x$ in the R–R case;

$\dfrac{\partial u}{\partial y} = 0$, $v = 0$, $\partial p/\partial y = \mathrm{Gr}\,T$, $T(x) = A - x$ in the R–F case;

left wall: $u = 0$, $v = 0$, $\partial p/\partial x = 0$, $T = A$;

right wall: $u = 0$, $v = 0$, $\partial p/\partial x = 0$, $T = 0$.

The dimensionless parameter τ_0 can be related to the Grashof number by the relation

$$\tau_0 = \frac{1}{\mathrm{Gr}}\frac{\beta g \Delta T H^2}{L c_s^2} = \alpha/\mathrm{Gr},$$

where α is very small. For example, for the thermal convective air flow at $\Delta T = 100°\mathrm{C}$ in a square cavity of $H = 1$ m, $\alpha \sim 3 \times 10^{-5}$. In simulations, the value of α should be taken from the interval $0 < \alpha \le 1$. In most computations, α was set equal to unity. Numerical experiments showed that a decrease in α resulted in a minor improvement of numerical accuracy, but the numerical algorithm became less stable, which required a reduction of the time step Δt. Thus, the terms containing τ_0 can be interpreted as regularizers in the context of the present analysis.

The problem of thermal convection in a rectangular cavity ($A = 4$) heated from the left was solved for moderate Grashof numbers at the low Prandtl number $\mathrm{Pr} = 0.015$ on a uniform 22×82 grid with the mesh size $h = 1/20$. In all cases, the time step was set equal to 10^{-6}.

In the R–R case at $\mathrm{Gr} = 4 \times 10^4$, the velocity and temperature fields computed at $\mathrm{Gr} = 3 \times 10^4$ were used as the initial conditions. In other computations, we used the unperturbed velocity and temperature fields as initial conditions.

In [11], four groups of methods for solving this problem were considered: finite-difference methods, finite-volume methods, finite element methods, and spectral methods. However, since the authors used a finite-difference approximation, the computed results were compared only with the numerical results obtained by finite-difference methods that were reviewed in [12].

In [13], the Navier–Stokes equations were written in the "streamfunction–vorticity formulation." The numerical procedure was based on the relaxation method. The idea of the method is that a time dependent term is added to the equation for streamfunction, which makes it a parabolic equation, and transient regularizers are added to the remaining equations. The difference equations were solved by the implicit scheme of the method of alternating directions (the ADI scheme). Time derivatives were approximated by upwind differences; spatial derivatives, by second-order accurate central differences. Most computations were performed on a uniform 81×321 grid.

In [14], the difference approximation of the Navier–Stokes equations written in the streamfunction–vorticity formulation was based on the Hermitian method for approximation of spatial derivatives, in which the first and second derivatives are treated as unknowns. The numerical solution was performed with the ADI scheme. The desired values of vorticity on the wall were calculated by means of the fourth-order accurate Hermitian relation. Several nonuniform grids that condensed toward the walls and in the regions of steep gradients were tested. Most solutions were obtained on a 41×121 grid.

In [15], the solution was obtained by the popular semi-implicit time-splitting method. In the semiexplicit approach, the explicit Adams–Bashforth method is applied to the nonlinear convective terms, and the implicit Crank–Nicolson method is applied to the viscous terms. In the spatial approximation, second-order accurate central differences were employed. All computations were performed on a uniform 25×97 grid.

In [16], the well-known AQUA (Advanced simulation using Quadratic Upstream differencing Algorithm) package was employed, based on second-order accurate upwind differences. The finite-difference equations were derived by the method of control volume. The resulting difference scheme was second order accurate in both time and space. Upwind differences were used to approximate the convective terms. The diffusive terms were approximated by second order accurate central differences. A uniform 21×81 grid was employed.

Comparing the results, one should keep in mind that, in contrast to the present analysis, the right wall of the cavity was heated in all studies cited here.

3.1. Numerical results for the R–R convection. The computations were performed for moderate Grashof numbers: $\mathrm{Gr} = 2 \times 10^4$, 3×10^4, and 4×10^4.

Table

Sourse	V^*	U^*	ψ^*
This work	0.448	0.672	0.409
[12]	0.452–0.482	0.669–0.704	0.406–0.409

For $\mathrm{Gr} = 2 \times 10^4$, we obtained a steady flow regime (see Fig. 1). The streamlines correspond to an elongated vortex. The results obtained are in good qualitative and quantitative agreement with those reported in [12, 13], where the flow was computed on very fine grids (on a 81×321 grid in [13]). Be-

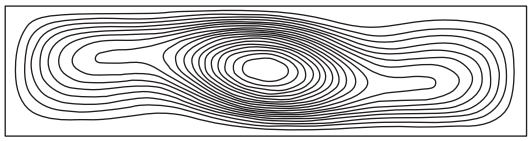

Fig. 1.

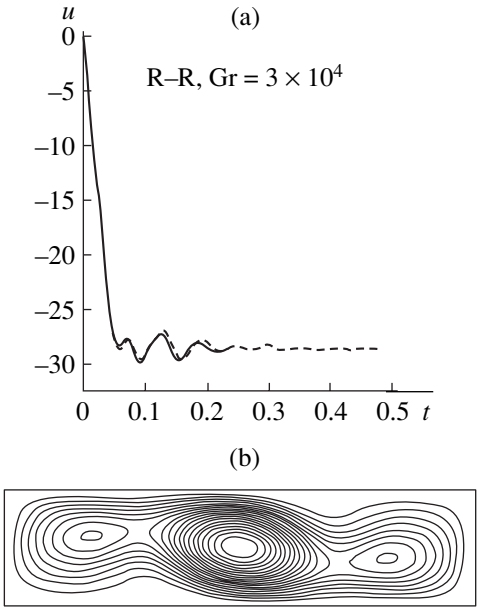

Fig. 2.

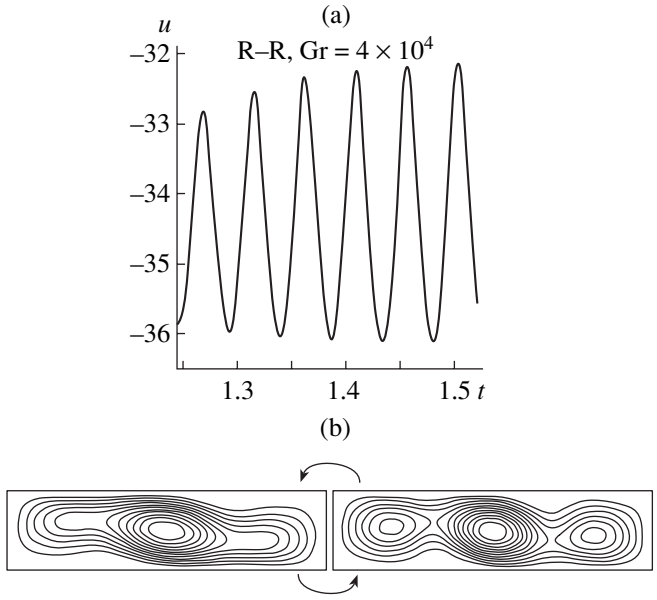

Fig. 3.

low, we compare the values of streamfunction and velocity components with those presented in [12], and the results turn out to be very close. Since a different nondimensionalization was used for velocity in [12], $u = \tilde{u}\,\nu \mathrm{Gr}^{0.5}/H$, $v = \tilde{v}\,\nu \mathrm{Gr}^{0.5}/H$, Table 1 compares the following quantities with the results from [12]:

$$\psi^* = \max_{xy}|\psi|/\mathrm{Gr}^{0.5},\ U^* = \max_{y}|u(y)|/\mathrm{Gr}^{0.5} \text{ for } x = 3A/4,\ V^* = \max_{x}|v(x)|/\mathrm{Gr}^{0.5} \text{ for } y = 1/2.$$

At $\mathrm{Gr} = 3 \times 10^4$, we obtained a steady flow regime (see Fig. 2), which is approached through oscillatory relaxation. Figure 2a compares the histories of the horizontal velocity at the center of the domain obtained for $\alpha = 1$ (solid curve) and $\alpha = 0.1$ (dashed curve). The curves are almost identical, which means that the solution weakly depends on the regularization parameter in the chosen interval of its values. In the majority of studies, oscillatory regimes were obtained in this case, but it was shown in [14, 15] that there exists a steady flow regime. The steady flow involves a main vortex located near the center and two additional vortices in the right and left parts of the cavity. In [15], a steady solution was obtained in this case, and its comparison with the results of the present study shows a good agreement. In particular, we compared the vertical profiles of horizontal velocity at $x = 3A/4$, the distributions of vertical velocity at $y = 1/2$, and streamline patterns.

At $\mathrm{Gr} = 4 \times 10^4$, we obtained an oscillatory flow regime (see Fig. 3) with an oscillation period estimated as $T_{\mathrm{vib}} = 0.047$ (Fig. 3a), which corresponds to the frequency $f_1 = 1/T_{\mathrm{vib}} = 21.28$. This result is very close to those reported in [12], where the results obtained by various authors were summarized. The oscillation frequency estimated by those authors varies from 21.186 to 22.35 in this case. In this problem, the flow has a structure similar to that obtained in the preceding case, and the oscillation involves variation of the vortex intensities, which is consistent with the results reported in [15].

3.2. Numerical results for the R–F convection. In contrast to the preceding case, a slip condition for the tangential velocity was set on the top boundary, which stimulates the oscillations.

At $\mathrm{Gr} = 10^4$, we obtained a steady flow regime (see Fig. 4), in which an asymmetric two-cell structure develops. The larger cell was located closer to the cool wall; the smaller one, between the cavity center and the hot left wall. The figures presented here are consistent with their counterparts presented in [16].

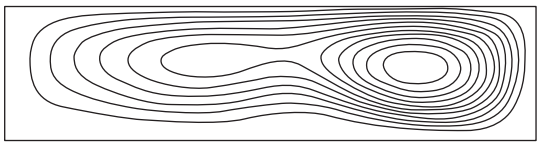

Fig. 4.

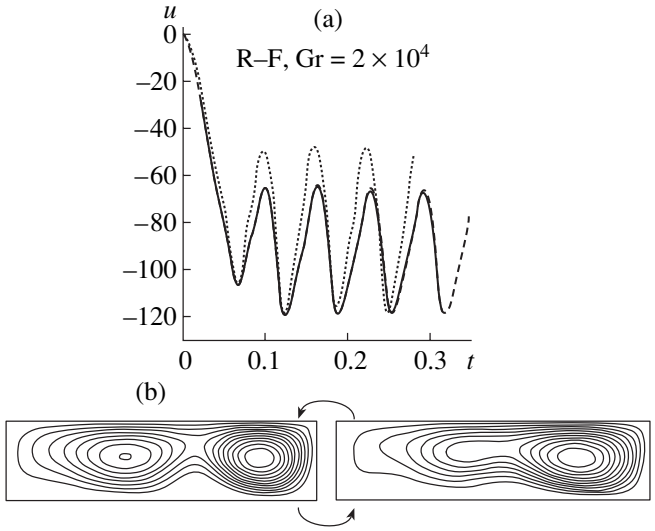

Fig. 5.

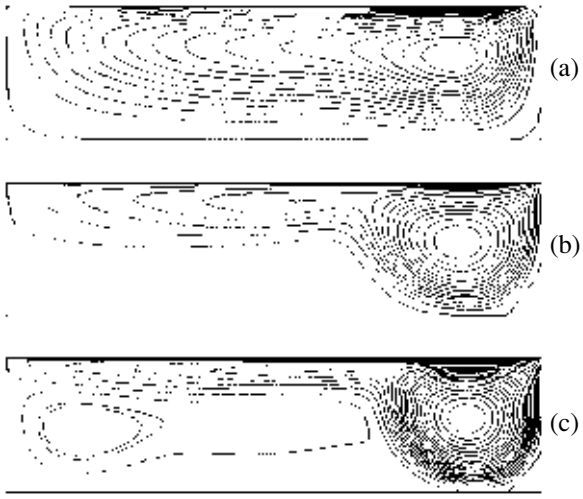

Fig. 6.

At $\mathrm{Gr} = 2 \times 10^4$, we obtained an oscillatory flow regime (see Fig. 5) with a period that can be estimated as $T_{\mathrm{vib}} = 0.0646$ (Fig. 5a), which corresponds to the frequency $f_1 = 15.48$. According to the review in [12], the oscillation frequency estimated by various authors varies from 15.580 to 17.2. In this problem, the flow is a vortex located closer to the right (cool) wall of the cavity. In the left part of the cavity, a weaker vortex develops (Fig. 5b). The oscillation involves variation of their intensities. In this case, we clearly see the evolution of the secondary vortices, whose pattern is consistent with the patterns shown in the corresponding figures in [16].

To elucidate the effect of the parameter α, this flow was computed for $\alpha = 1$ (solid curve) and $\alpha = 0.1$ (dashed curve); to check the accuracy, we computed the flow with $\alpha = 1$ on the refined 42×162 grid (dotted curve). The corresponding velocity histories are shown in Fig. 5a. It is obvious that a decrease in α does not affect the oscillation period and amplitude since the corresponding curves are practically identical. Condensation of the grid did not affect the oscillation frequency, but somewhat changed the oscillation amplitude.

4. MARANGONI CONVECTION

We now consider the problem of thermocapillary convection for a viscous incompressible fluid in the absence of gravity ($\mathbf{g} = 0$) (see [17, 18]). This problem was analyzed in numerous studies, because the liquid (melt) surface is free in various processes used in space technologies (e.g., directional crystallization or crucibleless zone melting), and it is the thermocapillary effect that gives rise to the convective flow in the melt.

The convective flow is due solely to surface tension, which is reflected by the following balance condition for the surface-tension and viscous-friction forces on the free top boundary: $\Pi_{yx} = (\partial\sigma/\partial T)\partial T/\partial x$, where $\sigma = \sigma(T)$ is the surface tension of the liquid.

In the two-dimensional case, according to (2)–(4), we have

$$\Pi = \eta\begin{bmatrix} 2\dfrac{\partial u}{\partial x} & \dfrac{\partial u}{\partial y} + \dfrac{\partial v}{\partial x} \\ \dfrac{\partial u}{\partial y} + \dfrac{\partial v}{\partial x} & 2\dfrac{\partial v}{\partial y} \end{bmatrix} + \tau\begin{bmatrix} u\left(\rho\left(u\dfrac{\partial u}{\partial x} + v\dfrac{\partial u}{\partial y}\right) + \dfrac{\partial p}{\partial x}\right) & u\left(\rho\left(u\dfrac{\partial v}{\partial x} + v\dfrac{\partial v}{\partial y}\right) + \dfrac{\partial p}{\partial y}\right) \\ v\left(\rho\left(u\dfrac{\partial u}{\partial x} + v\dfrac{\partial u}{\partial y}\right) + \dfrac{\partial p}{\partial x}\right) & v\left(\rho\left(u\dfrac{\partial v}{\partial x} + v\dfrac{\partial v}{\partial y}\right) + \dfrac{\partial p}{\partial y}\right) \end{bmatrix}.$$

Since $\partial p/\partial y$ and $v = 0$ on the top boundary, we have $\partial v/\partial x = 0$, and the tensor Π is simplified:

$$\Pi = \eta\begin{bmatrix} 2\frac{\partial u}{\partial x} & \frac{\partial u}{\partial y} \\ \frac{\partial u}{\partial y} & 2\frac{\partial v}{\partial y} \end{bmatrix} + \tau\begin{bmatrix} u\left(\rho u\frac{\partial u}{\partial x} + \frac{\partial p}{\partial x}\right) & 0 \\ 0 & 0 \end{bmatrix}.$$

Finally, we obtain the following dimensional condition on the top boundary: $\eta\partial u/\partial y = (\partial\sigma/\partial T)\partial T/\partial x$, which agrees with the conventional boundary condition in the thermocapillary convection problem for the Navier–Stokes equations. Note that $\partial\sigma/\partial T < 0$ for most liquids.

We considered the flow in a rectangular cavity of height H and length L. The flow was described by the set of equations (5) in which the extraneous force is eliminated. In the two-dimensional case, the equations are written as (7)–(10). We changed to dimensionless variables by means of the following formulas:

$$x = \tilde{x}H, \quad y = \tilde{y}H, \quad u = \tilde{u}\frac{\nu}{H}, \quad v = \tilde{v}\frac{\nu}{H}, \quad t = \tilde{t}\frac{H^2}{\nu}, \quad p = \tilde{p}\rho\left(\frac{\nu}{H}\right)^2, \quad T = \tilde{T}\Delta T.$$

With this nondimensionalization, we have the Marangoni number

$$\mathrm{Ma} = -\frac{\partial\sigma}{\partial T}\frac{\Delta T}{A}\frac{H}{\eta\chi},$$

$\mathrm{Re} = 1$; $\mathrm{Pr} = \nu/\chi$; $\tau_0 = \mathrm{M}^2$; and the Mach number $\mathrm{M} = \nu/(Hc_s)$, which is small in problems considered here.

Equations (8)–(11) is closed by setting the following boundary conditions:

bottom wall: $u = 0$, $v = 0$, $\partial p/\partial y = 0$, and $\partial T/\partial y = 0$;

top boundary: $\dfrac{\partial u}{\partial y} = -\dfrac{\mathrm{Ma}\,A}{\mathrm{Pr}}\dfrac{\partial T}{\partial x}$, $v = 0$, $\partial p/\partial y = 0$, and $\partial T/\partial y = 0$;

left wall: $u = 0$, $v = 0$, $\partial p/\partial x = 0$, and $T = 1$;

right wall: $u = 0$, $v = 0$, $\partial p/\partial x = 0$, and $T = 0$.

As in the thermal convection problem, the dimensionless parameter τ_0 can be related to the dimensional parameters of the problem as follows:

$$\tau_0 = \alpha\frac{\mathrm{Pr}}{\mathrm{Ma}\,A}, \quad \alpha = \left|\frac{\partial\sigma}{\partial T}\right|\Delta T\frac{1}{Hc_s^2}.$$

The value of α is very small. For example, for silicon at $\Delta T = 1000$°C in a cavity of height $H = 1$ cm, we have $\alpha \sim 10^{-9}$. In computations, the value of this parameter should be taken from the interval $0 < \alpha \le 1$. In computing the present problem, we set α equal to unity; accordingly, the terms containing τ_0 may be interpreted as regularizers.

The Marangoni convection problem in a rectangular cavity ($A = 4$) heated from the left was solved for $\mathrm{Ma} = 5$, 10, 20, 100, and 400 and $\mathrm{Pr} = 0.015$ on a uniform 27×102 grid. The time step was 5×10^{-6}. We used the unperturbed velocity and temperature fields as initial conditions.

The results computed for $\mathrm{Ma} = 400$ and $\mathrm{Ma} \le 100$ were compared with those reported in [17] and [18], respectively.

In [17], a new numerical technique based on the SOLA algorithm was developed, in which a finite-volume method was used on an orthogonal grid. Integration with respect to time was performed with the second-order accurate leap-frog explicit Euler scheme. Computations were performed on 25×100, 32×128, 40×160, and 50×200 grids.

In [18], a high-order accurate difference method was employed, in which spatial derivatives were approximated by second-order accurate central differences, a Hermitian scheme was used for streamfunction, the boundary conditions for vorticity were approximated with second-order accuracy, and the vorticity transport equation was solved by the method of alternating directions. The computations were performed on a nonuniform 35×95 grid.

Figure 6 shows the streamline patterns obtained for Ma = 5, 100, and 400. Since the Marangoni numbers are positive, the fluid motion along the top boundary is directed toward the cool wall. A vortex flow develops, whose center is closer to the right wall. With increasing Ma, the fluid velocity increases, and isotherms are distorted. At Ma = 100, additional vortices appear, whose sense of rotation is the same as that of the main vortex. The graphs presented in [18] for the same values of the Marangoni number are in good agreement

with these results. At Ma = 400, a vortex rotating counter to the main vortex forms in the lower left corner of the cavity. A similar pattern was obtained in [17]. The profiles of horizontal velocity computed at $x = A/2$ for various Marangoni numbers were compared with the corresponding profiles from [18]. For correct comparison, the velocity was calculated as $U^*(y) = u(y)\mathrm{Pr}/\mathrm{Ma}$, which corresponds to the nondimensionalization used in [18]. The graphs obtained are virtually identical with their counterparts presented in that paper.

Thus, the results obtained for Ma ≤ 100 and Ma = 400 are in good agreement with those reported in [18] and [17], respectively.

CONCLUSIONS

Unlike the Navier–Stokes equations, the QHD equations can be used to perform computations with simple explicit difference schemes on relatively coarse grids in a wide range of parameters. In all equations, spatial derivatives with respect to all coordinates are approximated by central differences characterized by second-order accuracy on uniform grids. Boundary conditions for the pressure described by Poisson's equation are obtained by setting the mass flux across the boundary of the computational domain equal to zero. The regularizers required to ensure stable computation at high Grashof and Marangoni numbers are provided by additional divergence terms containing a small parameter, which arise in the equations as a result of additional smoothing over time. The parameter τ_0 is a natural regularization parameter to be chosen as dictated by the specific problem.

The results computed for problems of low-Prandtl viscous incompressible flow on the basis of the QHD system are in complete agreement with those obtained by solving the Navier–Stokes equations. In addition to steady flow regimes, secondary (transient) regimes can be computed. It has been shown that the oscillation period is independent of the mesh size and regularization parameter.

Therefore, the QHD system of equations can be effectively used to simulate complex unsteady convective motion.

ACKNOWLEDGMENTS

This work was supported by the Russian Foundation for Basic Research, project no. 98-01-00155. It is our pleasure to thank B.N. Chetverushkin for helpful discussions and encouragement.

REFERENCES

1. Elizarova, T.G. and Chetverushkin, B.N., A Computational Algorithm for Gasdynamic Flows, *Dokl. Akad. Nauk SSSR*, 1984, vol. 279, no. 1, pp. 80–83.
2. Elizarova, T.G. and Chetverushkin, B.N., A Kinetic Computational Algorithm for Gasdynamic Flows, *Zh. Vychisl. Mat. Mat. Fiz.*, 1985, vol. 25, no. 10, pp. 1526–1533.
3. Antonov, M.A., Graur, I.A., Kosarev, L.V., and Chetverushkin, B.N., Numerical Simulation of Pressure Fluctuations in Three-Dimensional Cavities, *Mat. Modelirovanie*, 1996, vol. 8, no. 5, pp. 76–90.
4. Sheretov, Yu.V., Quasi-Hydrodynamic Equations as a Model of Compressible Viscous Heat-Conducting Flows, *Primenenie funktsional'nogo analiza v teorii priblizhenii* (Application of Functional Analysis in Approximation Theory), Sheretov, V.G. *et al.*, Eds., Tver: Tver. Gos. Univ., 1997, pp. 127–155.
5. Loitsyanskii, L.G., *Mekhanika zhidkosti i gaza* (Mechanics of Liquids and Gases), Moscow: Nauka, 1987.
6. Sheretov, Yu.V., On the Exact Solutions of Quasi-Hydrodynamic Equations, *Primenenie funktsional'nogo analiza v teorii priblizhenii* (Application of Functional Analysis in Approximation Theory), Andreeva, E.A. *et al.*, Eds., Tver: Tver. Gos. Univ., 1998, pp. 213–241.
7. Sheretov, Yu.V., A New Mathematical Model in Fluid Dynamics, *Primenenie funktsional'nogo analiza v teorii priblizhenii* (Application of Functional Analysis in Approximation Theory), Taiko, L.V. *et al.*, Eds., Tver: Tver. Gos. Univ., 1996, pp. 124–134.
8. Gurov, D.B., Elizarova, T.G., and Sheretov, Yu.V., Numerical Simulation of Fluid Flow in a Cavity Based on the Quasi-Hydrodynamic System of Equations, *Mat. Modelirovanie*, 1996, vol. 8, no. 7, pp. 33–44.
9. Elizarova, T.G., Kalachinskaya, I.S., Klyuchnikova, A.V., and Sheretov, Yu.V., Application of the Quasi-Hydrodynamic System of Equations in Simulations of Heat-Conducting Flows, *Trudy IV Mezhdunarodnoi konferentsii "Matematika, komp'yuter, obrazovanie"* (Proc. IV Int. Conf. "Mathematics, Computer, Education") Moscow, 1997, pp. 108–115.
10. *Biblioteka programm dlya resheniya setochnykh uravnenii* (Program Library for Solving Finite-Difference Equations), Nikolaev, E.S., Ed., Moscow: Mosk. Gos. Univ., 1984.
11. *Numerical Simulation of Oscillatory Convection in Low-Prandtl Fluids*, Roux, B., Ed., Braunschweig: Vieweg, 1990.

12. Behnia, M., Synthesis of Finite Difference Methods, in *Numerical Simulation of Oscillatory Convection in Low-Prandtl Fluids*, Roux, B., Ed., Braunschweig: Vieweg, 1990, pp. 265–272.
13. Behnia, M. and de Vahl Davis, G., Fine Mesh Solutions Using Streamfunction–Vorticity Formulation, in *Numerical Simulation of Oscillatory Convection in Low-Prandtl Fluids*, Roux, B., Ed., Braunschweig: Vieweg, 1990, pp. 11–18.
14. Ben Hadid, H. and Roux, B., Buoyancy-Driven Oscillatory Flows in Shallow Cavities Filled with a Low-Prandtl Number Fluid, in *Numerical Simulation of Oscillatory Convection in Low-Prandtl Fluids*, Roux, B., Ed., Braunschweig: Vieweg, 1990, pp. 25–34.
15. Biringen, S., Danabasoglu, G., and Eastman, T.K., A Finite-Difference Method with Direct Solvers for Thermally-Driven Cavity Problems, in *Numerical Simulation of Oscillatory Convection in Low-Prandtl Fluids*, Roux, B., Ed., Braunschweig: Vieweg, 1990, pp. 35–42.
16. Ohshima, H. and Ninokata, H., Numerical Simulation of Oscillatory Convection in Low Prandtl Number Fluids Using AQUA Code, in *Numerical Simulation of Oscillatory Convection in Low-Prandtl Fluids*, Roux, B., Ed., Braunschweig: Vieweg, 1990, vol. 27, pp. 90–97.
17. Ohnishi, M., Azuma, H., and Doi, T., Computer Simulation of Oscillatory Marangoni Flow, *Acta Astronaut*., 1992, vol. 26, nos. 8–10, pp. 685–696.
18. Roux, B., Ben Hadid, H., and Laure, P., Hydrodynamical Regimes in Metallic Melts Subject to a Horizontal Temperature Gradient, *Eur. J. Mech. B: Fluids*, 1989, vol. 8, no. 5, pp. 375–396.